Multiphoton excitation and ionization by elliptically polarized, intense short laser pulses: Recognizing multielectron dynamics and doorway states in C_{60} vs Xe

I. Shchatsinin, H.-H. Ritze, C. P. Schulz,* and I. V. Hertel†
Max Born Institute, Max-Born-Str. 2a, D-12489 Berlin-Adlershof, Germany
(Received 9 March 2009; published 15 May 2009)

Ionization and fragmentation of C_{60} fullerenes are studied by time-of-flight mass spectrometry, in elliptically polarized femtosecond laser fields at 797 nm of intensities $I_0=(0.5–4.3)\times10^{14}$ W cm^{-2}. Xe atoms serve as a test case. We derive a qualitative theory describing such polarization studies. It turns out that polarization dependence can very sensitively distinguish single active electron (SAE) and multiple active electrons dynamics. In the case of Xe a clear signature of SAE dynamics is observed, with very pronounced changes in the ion yield as a function of ellipticity, indicative of $\mathcal{N}=5–8$ and 18–22 photon processes for Xe^+ and Xe^{2+}, respectively. In contrast, only a moderate polarization dependence is observed in the C_{60} case, although at least 5 $h\nu$ photons at 797 nm are needed to generate C_{60}^+ and additional 11 for C_{60}^{2+}. At lower intensities, a moderate reduction in the ion yield for circular polarization establishes a two-photon SAE absorption process, connected with the key role of the lowest unoccupied molecular orbital (LUMO)$+1(t_{1g})$ as "doorway state." The absence of any polarization effect at 399 nm corroborates this finding. At high intensities enhanced fragmentation is observed, which is tentatively attributed to returning loops of electron trajectories by the combined action of the C_{60}^+ field and the circularly polarized laser field—in contrast to conventional wisdom that linear polarization should lead to an enhanced recolliding electron yield. No sign of a pronounced multiphoton polarization signature with five and more photons is seen for C_{60} which would be predicted by the SAE picture—although the slopes of the ion yield as a function of intensity are given by the corresponding power laws $\propto I_0^{\mathcal{N}}$. This is taken as clear evidence of multielectron dynamics after reaching the doorway state.

DOI: 10.1103/PhysRevA.79.053414 PACS number(s): 32.80.Rm, 33.20.Xx, 33.80.Rv, 42.50.Hz

I. INTRODUCTION

Interaction of intense ultrashort laser pulses with polyatomic molecular systems and the ensuing competition between ionization and fragmentation is a subject of considerable current interest (see, e.g., [1–3]). With its unique highly symmetric structure and its large number of electronic and nuclear degrees of freedom, C_{60} fullerene has proven to be a particularly instructive model for studying such processes. Various experimental studies and model calculations have been devoted in the past to a detailed understanding of its dynamics in intense laser pulses (see [4], and references given there). Recent theoretical work underlines the continuing attraction of the subject [5–10]. A broad variety of interesting phenomena have been discovered such as a massive change in the ionization patterns when the pulse duration is varied from a few femtoseconds to the picosecond range [11,12], above-threshold ionization (ATI) for short pulses [11], thermionic emission [13,14], population of Rydberg states [15,16], and excitation of giant breathing motion [17] as well as characteristic changes in ionization yields and relaxation times [18,19]. High-harmonic generation by C_{60} in intense laser pulses is also of interest [10].

Many studies with large molecules have focused on the yield of specific ions and fragments as a function of laser-pulse intensity. In the case of C_{60} many photons are typically absorbed when a femtosecond laser pulse interacts with it. This is a prerequisite for the observed characteristic patterns in mass spectra, consisting of multiply charged C_{60}^{q+}, some small fragments typically below C_{12}^+, and a substantial amount of multiply charged fullerenelike fragment ions C_{60-2m}^{q+}. The last are formed on a nanosecond and microsecond time scale (i.e., long after the interaction of the system with the laser pulse is over) from ensembles of very hot C_{60}^{q+} (created during the pulse) by sequential evaporation of several C_2 units. To allow, e.g., the appearance of C_{50}^{3+} about 120 eV of energy is needed, equivalent to ~80 photons at the fundamental Ti:sapphire wavelength. The role of intermediate states in the initial process of energy deposition in large molecules has been addressed in various contexts (see, e.g., [20]). For C_{60}, several pieces of experimental evidence as well as theoretical model simulations indicate that the t_{1g} state plays a crucial role as "doorway state" [1] in the excitation mechanism, followed by coupling to electronic and vibrational degrees of freedom. The t_{1g} orbital can be excited through the first dipole-allowed highest occupied molecular orbital (HOMO) $(h_u)\rightarrow$lowest unoccupied molecular orbital (LUMO)$+1(t_{1g})$ transition [21] by one blue photon ($\lambda\simeq400$ nm) or alternatively by two infrared photons [22,23] ($\lambda\simeq800$ nm). The selective relevance of an intermediate state is also corroborated by experiments with C_{60} in intense femtosecond pulses at much longer wavelengths $\lambda\geq1500$ nm where no such resonances can be accessed. Consequently mostly intact C_{60}^{q+} ions with charge states of up to $q=12$ were observed and only very few C_{60-2m}^{q+} fragments [24,25]. However, these fragments were found to be significantly more abundant when using linearly rather than circularly polarized light, which was seen as evidence of electron recollision playing an important role in vibrational

*cps@mbi-berlin.de
†Also at Department of Physics, Freie Universität Berlin, Arnimallee 14, 14195 Berlin, Germany. hertel@mbi-berlin.de

excitation of the C_{60}^{q+} ions—at these long wavelengths (quasistatic regime). The Keldysh parameter [26] $\gamma=\sqrt{W_I/2U_p}$ used there was 0.2, implying a ponderomotive potential $U_p=95$ eV$\propto I_0\lambda^2$ (I_0 being the laser intensity and $W_I=7.6$ eV being the ionization potential of C_{60}). Hence, energies of the rescattered electrons of up to $3.17U_p=300$ eV or even more are encountered in this process that can safely be described by a single active electron (SAE) [6]. For shorter wavelengths U_p is typically much smaller and the ionization process is more complex due to competition between multiphoton ionization (MPI), tunneling, excitation of intermediate electronic states, and nonadiabatic multielectron dynamics (NMED).

Apart from [25] and one pioneering study at particularly high intensities [27], only little is known about the role of ellipticity in the energy deposition process during the interaction of intense laser pulses with large molecular systems or clusters. In a recent letter [28] we presented first results of a study addressing this very aspect in ionization and fragmentation of C_{60} by femtosecond pulses of $\simeq$797 and 399 nm. While the influence of polarization on high-order harmonic generation (HHG) and ATI is well understood [29,30], only a few systematic experimental studies about ellipticity in strong-field ionization have been concerned with "recollision" and nonsequential double ionization (NSDI) of atoms [29,31,32]. Typically, a reduction in ion and HHG yield is attributed to the recolliding electron being driven away from its origin by circularly as opposed to linearly polarized light. If multiphoton absorption dominates, special angular momentum selection rules may also be significant. As to molecules, aside from C_{60}, mainly some special cases have been investigated, such as D_2 [33] and anthracene [34], where the angle between laser field and induced dipole moment may change in each of several multiphoton steps so that circular polarization can even enhance specific fragmentation channels. From a theoretical perspective, the generalization of advanced concepts "to an elliptically polarized field is extremely demanding if not impossible" [35]. Hence, investigations of such phenomena for a highly symmetric molecule may provide a fruitful testing ground.

The present paper extends our first studies of the subject [28] and tries to develop a theoretical model for analyzing the experimental observations. Key questions are whether a particular signature of the doorway state can be found and/or whether here, too, recollision effects can be identified. The paper is structured as follows. In Sec. II we describe the crucial experimental aspects and introduce our key observations. As a specific test case we study single and double ionizations of Xe as functions of ellipticity and laser-pulse intensity. In Sec. III a theoretical model is developed, starting with a simple "classical" field averaging, and rationalizing it then by quantum-mechanical considerations. We specifically address the differences of a single active chromophore in such polarization studies (SAE picture) as opposed to a multichromophore situation where several electrons can absorb photons (the basis for NMED). We then apply the model to the Xe test case and find surprising agreement with the experimental data. In Sec. IV we present and discuss the experimentally observed ion yields as a function of ellipticity and intensity for C_{60}^{q+} and the corresponding fullerenelike fragments C_{60-2m}^{q+}. Clear evidence of the role of the doorway state will be presented. We also demonstrate that such ellipticity studies—in contrast to mere ion yield measurements—allow indeed directly addressing the role of NMED vs SAE, the former dominating the energy deposition into C_{60} after the doorway state has been reached. Finally, we discuss some counterintuitive trends observed in the fragment ion yields for circularly polarized light by performing classical trajectory studies of the recolliding electrons under the combined action of the light field and the C_{60} potential. In Sec. V a short summary will conclude the paper.

II. EXPERIMENT

A. Setup and procedure

The experimental setup consists of a C_{60} molecular beam, a reflectron time-of-flight (ReTOF) mass spectrometer, and a commercial laser system. The C_{60} molecular beam is produced by evaporation of gold-grade C_{60} powder in an oven heated to 750 K. The laser beam is focused by an $f=50$ cm concave mirror perpendicular to both the effusive molecular beam and the spectrometer axis. The confocal length is then $\simeq$40 mm, much wider than the width of the C_{60} beam so that we operate with a cylindrical detection volume. The ions created in the intersection volume are extracted by a static electric field (Wiley-McLaren configuration), and directed by the ReTOF mass spectrometer onto multichannel plates. A detailed description of the ReTOF including voltage settings is given in a previous paper [16]. Recently, we have replaced the then-used multichannel scaler by an analog-to-digital converter card (Acqiris), which registers the amplified signal from the multichannel plates.

The mode-locked Ti:sapphire femtosecond laser used in this study consists of an oscillator (Femtosource Scientific PRO, Femtolasers) pumped by a 5 W Nd:YAG laser (Millennia V, Spectra-Physics) and a multipass amplifier (Femtosource Omega PRO, Femtolasers) pumped by a 13 W Nd:YLF laser (JADE, Thales Lasers). It delivers 797 nm pulses of $t_{1/2}=27$ fs duration with a bandwidth of 45 nm [full width at half maximum (FWHM)] at 1 kHz repetition rate. The laser-pulse duration is determined by a frequency resolved optical gating (FROG) measurement and is given here at FWHM of a Gaussian fit to the recorded intensity. The pulse energy is determined by a pyroelectric laser energy meter (TPM-300CE, Gentec Electro-Optics, Inc.). The maximum available pulse energy is about 800 μJ. The beam profile is derived from knife edge measurements, giving a beam waist $w=72$ μm (radius at $1/e^2$ maximum intensity of a Gaussian radial beam profile). The laser intensity is controlled by an attenuator (Altechna) consisting of a $\lambda/2$ plate and two thin-film polarizers. Second-harmonic radiation at 399 nm can be generated by a 100 μm beta barium borate (BBO) crystal. The pulse intensities I_0 given in the present work refer to the cycle-averaged maximum in space and time (both Gaussian profiles).

The ellipticity of laser pulses is changed by rotating a zero-order $\lambda/4$ plate (aperture, 1.45 cm; B. Halle). This plate consists of two quartz plates with a difference in thickness of $\lambda/4$, which are assembled with crossed crystal axes. The

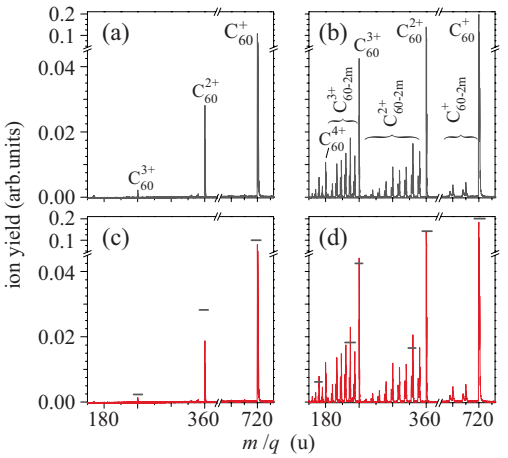

FIG. 1. (Color online) Examples of mass spectra from C_{60} after excitation with 27 fs pulses at 797 nm. (a) and (b) originate from linearly polarized light; (c) and (d) from circularly polarized light. The low-intensity mass spectra [(a) and (c)] have been taken at $I_0 = 0.94 \times 10^{14}$ W cm^{-2}; the high-intensity ones [(b) and (d)], at 4.08×10^{14} W cm^{-2}. The small horizontal lines in (c) and (d) indicate the peak maxima in (a) and (b), respectively.

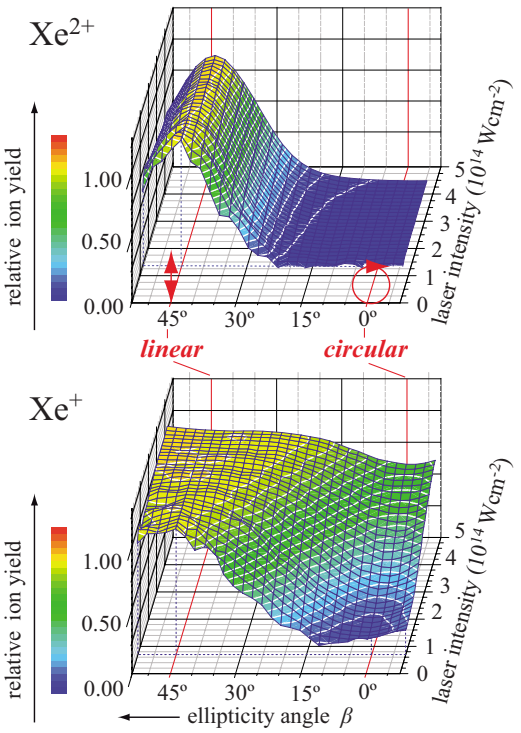

FIG. 2. (Color online) Xe^+ and Xe^{2+} ion yields as functions of ellipticity angle β obtained with 27 fs laser pulses at 797 nm. The polarization changes from linear (β=45°) to circular (β=0°). The ion yield is normalized at each intensity [I_0=(0.65–4.3) $\times 10^{14}$ W cm^{-2}] to its value for linear polarization. Note the dramatic reduction in ion signal, especially for Xe^{2+}, when the polarization changes from linear to circular.

total thickness is approximately 0.16 cm, and no significant pulse lengthening has been observed at 797 nm in the measured autocorrelation. At the beginning of an experimental cycle the position of linear polarization (denoted here by $\vartheta = 0°$) was determined by maximizing the second-harmonic signal from a BBO crystal. In this case the fast axis of the $\lambda/4$ plate was perpendicular to polarization axis of the incident laser beam. During the measurements the $\lambda/4$ plate was rotated counterclockwise from $\vartheta = -8.8°$ to 52.8° in steps of 2.2°. Due to our choice of the initial orientation of the fast axis, right-hand circularly (RHC) polarized (σ^-) light is produced at $\vartheta = 45°$. It should be noted here that the rotation of the $\lambda/4$ plate not only changes the ellipticity of laser light but also rotates the alignment angle δ of the main axis of the polarization ellipse with respect to the mass-spectrometer axis. This is, however, of no significance for the results on multiply charged C_{60} and fullerenelike fragments presented in this paper which do not depend on δ. In principle, one can avoid this by using a combination of a rotatable $\lambda/2$ plate and a fixed $\lambda/4$ plate.

B. Mass spectra

Mass spectra are accumulated over 5000 laser shots for each intensity and ellipticity, which are repetitively modulated many times to average over fluctuations. Figure 1 shows typical mass spectra of C_{60} taken with linearly polarized light at two different intensities, 0.94×10^{14} and 4.08×10^{14} W cm^{-2} (upper row), and with circular polarization and the same two intensities (lower row). Figures 1(a) and 1(b) reproduce the well-known mass spectra when C_{60} is excited and ionized with short (27 fs) linearly polarized laser pulses: at intensities below 1×10^{14} W cm^{-2} intact C_{60}^{q+} ions are observed with charge states $q \leq 3$, while for higher intensities fullerenelike fragments (C_{60-2m}^{q+}) appear in the mass spectrum, especially for $q \geq 2$ [18]. At first glance, the mass spectra shown in Figs. 1(c) and 1(d) taken with circularly polarized laser pulses look very similar. A closer inspection shows, however, small but significant differences as indicated by the small horizontal bars on top of the mass peaks in Figs. 1(c) and 1(d), representing the respective signals in Figs. 1(a) and 1(b). At lower intensities the ions' signal decreases by approximately 25% when changing the polarization from linear to circular, best noticeable when comparing the C_{60}^{2+} mass peak in Figs. 1(a) and 1(c). On the other hand, by comparing Figs. 1(b) and 1(d) one finds that for high intensities the ion signals of the fullerenelike fragments even increases by up to 20% when circularly polarized light is used, while the ion signal of the intact C_{60}^{q+} ions is almost unchanged. These first qualitative inspections already hint at interesting effects of the laser intensity and ellipticity on the excitation and ionization process in complex systems.

C. Multiphoton single and double ionizations of Xe

As experimental test cases we have first studied the dependence of the multiphoton ionization and double ionization of Xe. The ion yield as a function of intensity (over several orders of magnitude) has been studied some time ago in very careful benchmark type of study [36,37]. We have found, however, no polarization-dependent investigation in the literature.

Our results are shown in Fig. 2 in a three-dimensional

(3D) plot as a function of intensity and ellipticity angle $\beta = 45° - \vartheta$, the latter being determined by the alignment angle ϑ of the $\lambda/4$ plate as described above (we will come back to the definition of β in Sec. III). For clarity we report here and in the following the ion yield normalized to the signal for linear polarization ($\beta = 45°$), keeping in mind that according to [36,37] the absolute ion yield increases by orders of magnitudes over the intensity range displayed in Fig. 2. What we see is a dramatic decrease in the ion signals at all intensities when the polarization is changed from linearly to circularly polarized light. Some reduction in this trend is recognized for higher intensities where saturation intensities for the ion signals have been reached. These experimental findings warrant a somewhat detailed theoretical discussion before continuing with the main subject of this work on C_{60}.

III. MULTIPHOTON EXCITATION WITH ELLIPTICALLY POLARIZED LIGHT

It is important to point out that we do not claim here to develop a general theory for excitation and ionization by intense elliptically polarized laser pulses. This can only be derived in a detailed system-specific numerical computation which would go far beyond the scope of the present paper. However, we will try to obtain some physical insights into the origin of differences between linearly and circularly polarized light in such processes and develop a simple model for a qualitative approach to the analysis of ellipticity-dependent strong-field ionization yields for large finite systems.

For the low-intensity (perturbative) limit and for specific examples of simple atoms, a theoretical treatment of the differences between two- and three-photon ionizations by linearly and circularly polarized laser light was first reported as early as 1972 by Lambropoulos [38]. He found that under certain conditions circularly polarized light can be more efficient, but also the opposite is possible. Others generalized this observation [39,40], but Reiss [41] showed first that for higher-order processes circularly polarized light would in general lead to smaller cross sections. The latter statement is obviously in agreement with our observation for Xe described above, where up to eight photons are involved in the first ionization step. None of these calculations has so far produced a general formula for the dependence of ionization cross sections as a function of ellipticity ϵ and number $\mathcal{N}$ of photons involved. We note in passing that a somewhat related problem has been discussed for the generation of the $\mathcal{N}$th-order high harmonics with elliptically polarized light [42,43]. However, the often-used formula

$$\sigma_{HHG}^{(\mathcal{N})} \propto \left(\frac{1-\epsilon^2}{1+\epsilon^2}\right)^{\mathcal{N}-1} \tag{1}$$

is obviously not applicable in the context of ionization: it predicts zero yield for circular polarization ($\epsilon = 1$) in any order process, which contradicts the experimental evidence for ionization processes.

Such a general formula cannot certainly be derived exactly, but one may hope to find an approximate answer for large-$\mathcal{N}$ and/or large finite systems. We will first offer what we call a quasi-"classical formula" and we will then look for a quantum-mechanical rationalization. In doing so, we will focus on the angular momentum part of the wave functions of initial, intermediate, and final states involved, which we consider the key for understanding the response of the system to intense elliptically polarized light pulses, and ignore the radial parts for the sake of simplicity. We note in this context that in strong-field ionization theory (so-called strong-field approximation (SFA), first formulated by Reiss [44]; see also [23] for a summary and application to C_{60}), only knowledge of the initial momentum space wave function of the target enters into the calculation of ion yields.

Before going into details, we recall that—at not too high intensities—the transition rate (in units of s^{-1}) for an $\mathcal{N}$-photon excitation or ionization process from state $|a\rangle$ to $|b\rangle$ is given by

$$R_{ba}^{(\mathcal{N})} = \sigma_{ba}^{(\mathcal{N})} \Phi^{\mathcal{N}} \propto I_0^{\mathcal{N}}, \tag{2}$$

where I_0 is the laser intensity (averaged over one cycle, at a given position in space), $\Phi = I_0/\hbar\omega$ is the photon flux, and ω is the angular frequency of the radiation. The energy of the $\mathcal{N}$ photons absorbed has to be in resonance with the transition energy,

$$\hbar\omega_{ba} = \mathcal{N}\hbar\omega, \tag{3}$$

and the so-called generalized (multiphoton) cross section $\sigma_{ba}^{(\mathcal{N})}$ is a constant in $\mathcal{N}$th-order perturbation theory—its units being $[\sigma^{(\mathcal{N})}] = m^{2\mathcal{N}} s^{\mathcal{N}-1}$. Intensity dependence (2) is well known to give a good quantitative description of ionization rates for atoms and molecules, including C_{60}, and to allow for an estimate of the number of photons involved—as long as I_0 is sufficiently below saturation intensity, where its breakdown due to tunneling and above barrier ionization is often difficult to even discern from geometrical effects due to the spatial intensity distributions of realistic laser beams. Equation (2) thus forms the basis for the following considerations.

A. Description of elliptically polarized light

As we aim at a unified expression for elliptically polarized light (rather than two independent expressions for linearly and circularly polarized light), we find it most convenient (following, e.g., Ref. [45]) to express the unit polarization vector for the most general (fully coherent) elliptically polarized light by

$$\vec{e} = e^{-i\delta}\cos\beta\,\vec{e}_{+1} - e^{i\delta}\sin\beta\,\vec{e}_{-1}, \tag{4}$$

where δ is the alignment angle of the polarization ellipse with respect to a given x axis, and β is an angle determining the ellipticity—with special cases $\beta = 0$, $\pi/4$, and $\pi/2$ for left-hand circularly (LHC) (or σ^+), linearly (π), and RHC (or σ^-) polarized light, respectively. The unit polarization vectors $\vec{e}_{+1}$ and $\vec{e}_{-1}$ refer to σ^+ and σ^- light, respectively, propagating into the $+z$ direction. We note that in this *helicity basis* $\vec{e}_{+1}$ and $\vec{e}_{-1}$ represent photons with a spin = 1 and projection quantum numbers $q = +1$ and -1, respectively, and are orthonormal complex quantities for which

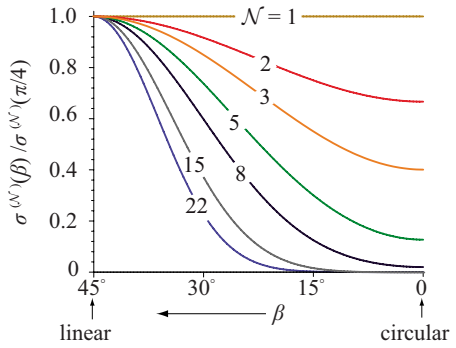

FIG. 3. (Color online) Dependence of the generalized relative $\mathcal{N}$-photon cross section on the ellipticity angle β for different numbers of $\mathcal{N}$, normalized to its value for linearly polarized light, $\beta=\pi/4$.

$$\vec{e}_q\vec{e}^{\,*}_{q'}=\delta_{qq'} \quad \text{and} \quad \vec{e}^{\,*}_{+1}=\vec{e}_{-1} \tag{5}$$

hold. When elliptically polarized light is created as described in Sec. II by rotating a $\lambda/4$ plate, the ellipticity angle $\beta=\pi/4-\vartheta$ is directly related to the rotation angle ϑ with respect to linear polarization. For reference we note that β relates to the often-used ellipticity ϵ (ratio of minimum to maximum of the polarization ellipse) as

$$\epsilon=\cot(\beta+\pi/4).$$

The *real* electric field vector for this elliptically polarized light at a given point in space is then (apart from an arbitrary phase factor defining time $t=0$)

$$\vec{E}(\vec{r},t)=\frac{i}{2}E_0(\vec{e}e^{-i\omega t}-\vec{e}^{\,*}e^{i\omega t}), \tag{6}$$

with the angular (carrier) frequency ω of the light, and the field amplitude E_0. With the vacuum resistance $Z_0=(\epsilon_0 c)^{-1}=376.7\ \Omega$ the corresponding time dependence of the light intensity is

$$I(t,\beta)=-\frac{E_0^2}{4Z_0}[\vec{e}e^{-i\omega t}-\vec{e}^{\,*}e^{i\omega t}]^2=I_0[1-\sin(2\beta)\cos(2\omega t)], \tag{7}$$

where we have made use of Eq. (5). It is important to realize that one key difference between linearly and circularly polarized light is the temporal behavior of its instantaneous intensity $I(t)$: for linearly polarized light $[\sin(2\beta)=1]$ it varies from $0\le I(t)\le 2I_0$, while for circularly polarized light $[\sin(2\beta)=0]$ it is constant with time $I(t)\equiv I_0$. Note that the time-averaged intensity $\langle I(t)\rangle=I_0=E_0^2/2Z_0$ is *independent* of the polarization state. Hence, in *single-photon absorption* the excitation probability which depends linearly on intensity is *independent of polarization* for isotropic targets. In contrast, it is intuitively plausible that for multiphoton excitation which depends according to Eq. (2) on the $\mathcal{N}$th power of the intensity, this will be reflected in multiphoton transition cross sections.

B. "Classical" intensity averaging

While it is clear that the excitation probability in a multiphoton process will not directly follow the rapid intensity changes with time described by Eq. (7) during a single period of the light oscillation, from a classical viewpoint one expects—if Eq. (2) is valid—that the *overall* transition rate in an $\mathcal{N}$-photon process will depend on the *time average* of the intensity $\langle I^{\mathcal{N}}(t,\beta)\rangle$. Using tabulated expressions for definite integrals [46], we obtain

$$\langle I^{\mathcal{N}}(t,\beta)\rangle=I_0^{\mathcal{N}}\frac{\omega}{2\pi}\int_0^{2\pi/\omega}[1-\sin(2\beta)\cos(2\omega t)]^{\mathcal{N}}dt \tag{8}$$

$$=I_0^{\mathcal{N}}\sum_{\mathcal{K}=0}^{\mathcal{N}}\binom{\mathcal{N}}{\mathcal{K}}^2\sin^{2\mathcal{K}}\beta\cos^{2\mathcal{N}-2\mathcal{K}}\beta \tag{9}$$

$$=I_0^{\mathcal{N}}\cos^{\mathcal{N}}(2\beta)P_{\mathcal{N}}\left(\frac{1}{\cos(2\beta)}\right), \tag{10}$$

with the Legendre polynomials $P_{\mathcal{N}}(x)$. The generalized multiphoton cross section is thus expected to depend on the ellipticity angle β. In a direct $\mathcal{N}$-photon transition according to Eq. (3), this β-dependent cross section $\sigma_{ba}^{(\mathcal{N})}(\beta)$ will be largest for linear polarization ($\beta=\pi/4$) since the instantaneous intensity variation is largest, and it will become a minimum for circular polarization ($\beta=0$ or $\pi/2$) where it is constant with time $I(t)=I_0$. For comparison we normalize to linear polarization (which is what typically is reported in the literature) and obtain in this "classical averaging" model

$$\sigma_{ba}^{(\mathcal{N})}(\beta)=\sigma_{ba}^{(\mathcal{N})}(\pi/4)\frac{\langle I^{\mathcal{N}}(t,\beta)\rangle}{\langle I^{\mathcal{N}}(t,\pi/4)\rangle}, \tag{11}$$

which replaces $\sigma_{ba}^{(\mathcal{N})}$ in Eq. (2). For several values of $\mathcal{N}$ this is illustrated in Fig. 3 as a function of β in the range from $\simeq\pi/4$ (linear polarization) to $\simeq 0$ (circular polarization). For later use, we give for $\mathcal{N}=2$ the explicit expression originating from Eq. (9),

$$\frac{\sigma_{ba}^{(2)}(\beta)}{\sigma_{ba}^{(2)}(\pi/4)}=\frac{\langle I^2(t,\beta)\rangle}{\langle I^2(t,\pi/4)\rangle}=\frac{5-\cos(4\beta)}{6}, \tag{12}$$

which shows the smoothest drop among the curves shown in Fig. 3 from 1 to 2/3.

In summary, the classical averaging predicts a *drop* in the *effective multiphoton cross section* between linear and circular polarizations—a direct consequence of the fact that the electric field vector for circularly polarized light is constant but only $1/\sqrt{2}$ of that for the maximum of linearly polarized light. This drop in the strong-field ionization cross section can be quite dramatic if the number $\mathcal{N}$ of photons involved is large—as we have indeed observed experimentally in the Xe^{2+} case (Fig. 8).

Unfortunately, we have not found any report in the literature which gives a numerical calculation of $\sigma_{ba}^{(\mathcal{N})}(\beta)$ as a function of ellipticity angle for a real system. For curiosity, however, we compare our formula with the ratio of circularly to linearly polarized light for multiphoton ionization of H atoms with 1064 nm calculated in the strong-field approxi-

mation by Reiss [47]. For this process involving at least $\mathcal{N}=12$ photons, our formula predicts $\sigma_{ba}^{(12)}(0)/\sigma_{ba}^{(12)}(\pi/4)=1.5\times10^{-3}$, which is exactly the value Reiss found at $I_0=4\times10^{13}$ W cm^{-2}, while his value decreases at lower intensities and rises up to a maximum of 0.015 at 5×10^{14} W cm^{-2}—corresponding to $\mathcal{N}=8-9$ when using our formula. This gives us some confidence that we can at least describe trends at such intermediate intensities below saturation.

C. Angular momentum transfer for a single-electron system

As we shall see, formula (9) and (10) provides indeed excellent fits to the experimental observations in the present work and thus may be used for a first inspection of such type of data. As a general rule, classical field approximations of the type used in Sec. III B tend to describe the action of electromagnetic radiation field well for high field strengths—which is, as we have seen, corroborated to some extend by SFA. If we want to understand the deeper quantum-mechanical reason for this dramatic difference between linearly and circularly polarized light in the ionization process, we have to focus our attention onto the angular momentum transferred during the photon absorption, remembering that ionization with $\mathcal{N}$ photons of circular polarization transfers $\pm\mathcal{N}\hbar$ of angular momentum to the target electrons, while with linear polarization no angular momentum transfer occurs. General polarization vector (4) used here allows description of both situations in a unified manner, expressing linearly polarized light as linear superposition of the two photon basis states for σ^+ and σ^- light.

To follow the individual steps for photon absorption (and angular momentum transfer), recall that within the *electric dipole approximation* the interaction Hamiltonian (written here in the length gauge) is characterized by transition matrix elements

$$\hat{T}_{ba}=\langle b|\vec{D}\cdot\vec{e}|a\rangle=D_{ba}\langle b|\hat{P}|a\rangle, \tag{13}$$

where $\vec{D}=e_0\vec{r}$ is the dipole operator, e_0 is the unit charge, $\vec{r}$ is the coordinate of the electron to be excited, and $\vec{e}$ is the polarization vector defined by Eq. (4). In the spirit of this general discussion we neglect all complications arising from the radial dipole transition matrix elements D_{ba} and ignore any resonance denominators arising in low-intensity perturbation theory of multiphoton processes [48]. We thus focus exclusively on the angular part, which we can write explicitly as

$$\begin{aligned}\langle b|\hat{P}|a\rangle&=\langle b|\hat{P}^+ + \hat{P}^-|a\rangle\\&=\langle l_b m_b|C_{11}e^{-i\delta}\cos\beta - C_{1\text{-}1}e^{i\delta}\sin\beta|l_a m_a\rangle.\end{aligned} \tag{14}$$

We consider here a single-active-electron system, characterized by its orbital angular quantum numbers lm (ignoring electron spin and any other angular momenta of the target). To conveniently evaluate the transition matrix elements, we have written $\vec{r}$ in helicity coordinates in analogy to the polarization vector $\vec{e}$, where $C_{1q}(\theta,\varphi)=\sqrt{4\pi/3}Y_{1q}(\theta,\varphi)$ are the so-called renormalized spherical harmonics. The components $\hat{P}^{\pm}$ for the σ^+ $(q=1)$ and σ^- $(q=-1)$ of the transition operator, which are given by

$$\hat{P}^+=-e^{-i\delta}\cos\beta\sin\theta e^{i\varphi}/\sqrt{2}, \tag{15}$$

$$\hat{P}^-=+e^{i\delta}\sin\beta\sin\theta e^{-i\varphi}/\sqrt{2}, \tag{16}$$

induce $\Delta m=+1$ and $\Delta m=-1$ transitions, respectively. Using the Wigner-Eckart theorem the matrix elements of C_{kq} can be expressed as (see, e.g., [45], p. 452, and following pages)

$$\langle l'm'|C_{kq}|lm\rangle=(-1)^{l'-m'}(2l'+1)^{1/2}\begin{pmatrix}l' & k & l\\ -m' & q & m\end{pmatrix}\langle l'||\mathbf{C}_k||l\rangle \tag{17}$$

in terms of $3j$ symbols and the reduced matrix element

$$\langle l'||\mathbf{C}_k||l\rangle=(-1)^{l'}\sqrt{(2l+1)}\begin{pmatrix}l' & k & l\\ 0 & 0 & 0\end{pmatrix} \tag{18}$$

in the notation of [49]. Note that $\langle l'm'|C_{1q}|lm\rangle$ is real but its sign depends on whether σ^+ $(q=1)$ or σ^- light $(q=-1)$ is active.

Guided by $\mathcal{N}$th-order perturbation theory, but focusing only on the angular part, we recall that the single-photon-absorption cross section is given by

$$\sigma_{ba}^{(1)}\propto\sum_{l_b m_b m_a}|\langle b|\hat{P}|a\rangle|^2, \tag{19}$$

where one has to average over all initial substates m_a and to sum over all final states $l_b m_b$. The angular part of the two-photon-absorption cross section is characterized by

$$\sigma_{ba}^{(2)}\propto\sum_{m_b m_a}\left|\sum_j\langle b|\hat{P}|j\rangle\langle j|\hat{P}|a\rangle\right|^2, \tag{20}$$

where the coherent summation over $j=l_j m_j$ includes in principle all dipole-allowed intermediate states and here, too, one finally has to average over initial states and to sum over final states.

For higher-order processes a similar product of transition matrix elements will be the key to the angular momentum transfer,

$$\sigma^{(3)}\propto\sum_{m_b m_a}\left|\sum_j\sum_h\langle b|\hat{P}|h\rangle\langle h|\hat{P}|j\rangle\langle j|\hat{P}|a\rangle\right|^2, \tag{21}$$

and so on. Based on the two-component nature of the transition amplitudes according to Eq. (14), the general structure of the transition pathways is illustrated in a very schematic manner in Fig. 4. Note that the intermediate ladder steps (dashed lines) are not real levels, but rather just indicate the type of transition amplitudes involved. In each photon-absorption step, only transitions with $\Delta l=\pm1$ and—due to our choice of the coordinate system—$\Delta m=\pm1$ participate, which leads to the rather transparent picture presented in Fig. 4. Of course, in a strict perturbation approach to the cross sections, one would have to consider resonance denominator and radial matrix elements in detail. However, since we are discussing ionization in intense laser fields, one may expect

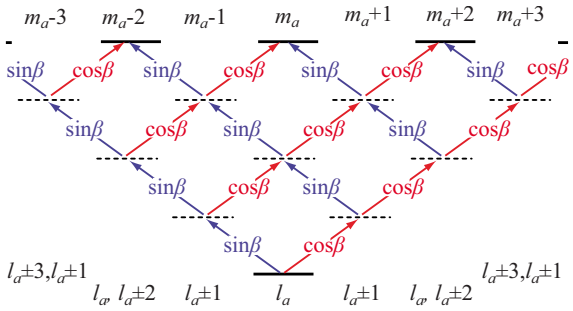

FIG. 4. (Color online) Schematic of multiphoton transitions (here $\mathcal{N}=4$) composed by one-photon amplitudes, which are $\propto\cos\beta$ for LHC polarized excitation ($\Delta m=+1$) and $\propto-\sin\beta$ for RHC polarized excitation ($\Delta m=-1$). Starting point is a ground state $|l_a m_a\rangle$. Note that the dashed horizontal lines just indicate intermediate total photon energies and do not necessarily coincide with real levels of the system.

the energetic and radial structure of intermediate levels to average out in the process of absorbing many photons. Similar to the explicit formulation of SFA approaches, the structure of intermediate wave functions thus does not enter into the final results.

1. Single-photon absorption

Before analyzing higher-order transitions in detail, it is instructive to first show explicitly in terms of the language used presently why Eq. (19) is independent of polarization. With Eqs. (14), (4), and (5) we evaluate $|\langle b|\hat{P}|a\rangle|^2$ by applying the selection rule $\Delta m=\pm 1$ and noting that *either* $m_b=m_a+1$ *or* $m_b=m_a-1$. Thus, products of matrix elements of the type $\langle b|C_{11}|a\rangle\langle b|C_{1\text{-}1}|a\rangle$ always vanish when summing over all m_b and m_a and the alignment angle δ of the polarization ellipse disappears, so that we finally have

$$\sum_{m_b m_a} |\langle b|\hat{P}|a\rangle|^2 = \sum_{m_b m_a} \{\cos^2\beta\langle b|C_{11}|a\rangle^2 + \sin^2\beta\langle a|C_{1\text{-}1}|b\rangle^2\}. \tag{22}$$

Using explicit expressions (17) for the matrix elements of C_{1q} and making use of the orthogonality relations of the $3j$ symbols, *single-photon-absorption cross section* (19) for an initial state with quantum numbers $\gamma_a l_a$ becomes

$$\sigma^{(1)} \propto \sum_{l_b} (2l_b+1)\langle l_b||\mathbf{C}_k||l_a\rangle^2 \tag{23}$$

and is indeed *independent* of the polarization.

2. Multiphoton absorption

We now evaluate the product sum squared of $\mathcal{N}$ matrix elements analogous to Eq. (20) and (21), which for an initial state $|l_a m_a\rangle$ can be written as

$$\sigma_{ba}^{(\mathcal{N})} \propto \sum_{l_b m_b m_a} \Big| \langle l_b m_b| \sum_{l_{\mathcal{N}-1} m_{\mathcal{N}-1}} \hat{P}|l_{\mathcal{N}-1} m_{\mathcal{N}-1}\rangle \times\langle l_{\mathcal{N}-1} m_{\mathcal{N}-1}|\cdots \sum_{l_j m_j} \hat{P}|l_j m_j\rangle\langle l_j m_j|\cdots \sum_{l_1 m_1} \hat{P}|l_1 m_1\rangle \times\langle l_1 m_1|\hat{P}|l_a m_a\rangle \Big|^2, \tag{24}$$

with $\hat{P}=\hat{P}^+ + \hat{P}^-$ as defined in Eqs. (15) and (16). Selection rules as indicated in the Pascal triangle in Fig. 4 are taken care of automatically in summations (24). We now identify

$$\sum_{lm} |lm\rangle\langle lm| = \hat{\mathbf{I}} \tag{25}$$

as unity operator and can thus write

$$\sigma_{ba}^{(\mathcal{N})} \propto \sum_{l_b m_b m_a} |\langle l_b m_b|(\hat{P}^+ + \hat{P}^-)^{\mathcal{N}}|l_a m_a\rangle|^2 = \sum_{m_a} \langle l_a m_a|(\hat{P}^+ + \hat{P}^-)^{\mathcal{N}}(\hat{P}^{+*} + \hat{P}^{-*})^{\mathcal{N}}|l_a m_a\rangle, \tag{26}$$

where in the last step we have used $|\langle b|\hat{O}|a\rangle|^2 = \langle a|\hat{O}^*|b\rangle\langle b|\hat{O}|a\rangle$ for the Hermitian operators $\hat{P}^\pm$, and once again unity operator (25).

We can now substitute Eqs. (15) and (16) into Eq. (26) to obtain

$$\sigma_{ba}^{(\mathcal{N})} \propto \sum_{m_a} \langle l_a m_a|[|C_{1\text{-}1}|^2\sin^2\beta + |C_{11}|^2\cos^2\beta - 2\,\mathrm{Re}(C_{11}^* C_{1\text{-}1} e^{2i\delta})\sin\beta\cos\beta]^{\mathcal{N}}|l_a m_a\rangle = \sum_{m_a} \langle l_a m_a|\sin^{2\mathcal{N}}\theta(1-\sin 2\beta\cos 2\phi)^{\mathcal{N}}|l_a m_a\rangle,$$

with $\phi=\varphi-\delta$. We see that, just as in SFA, only the initial wave function $|l_a m_a\rangle$ enters the final result. Integration over θ just gives a constant and all dependence on β is connected with the azimuthal angle. As expected from the physics, the alignment angle δ just changes the zero phase location and is without relevance when integrating φ over 2π. Thus we finally have

$$\sigma_{ba}^{(\mathcal{N})} \propto \frac{1}{2\pi}\int_0^{2\pi} (1-\sin 2\beta\cos 2\phi)^{\mathcal{N}} d\phi,$$

which is *identical* to *"classical" formula* (8)—Q.E.D. We even recognize directly that the time average there is now translated into an average over the azimuthal angle ϕ. The latter may be seen to represent the circular polarization of the light (i.e., the rotation of the electric field vector around the z axis).

Another way of looking at this is by seeing the matrix elements of $\hat{P}^\pm$ as transition amplitudes which, summed over all lm in each absorption step, are found to be identical in each step. Thus, we have to replace $\hat{P}^+ \to \cos\beta$ and $\hat{P}^- \to \sin\beta$, and the Pascal triangle in Fig. 4 allows one to count the number of different pathways for reaching a final m_b. Each of these product amplitudes depends on the number $\mathcal{K}$ of steps induced by $\hat{P}^-$ ($\Delta m=-1$) and on the corresponding

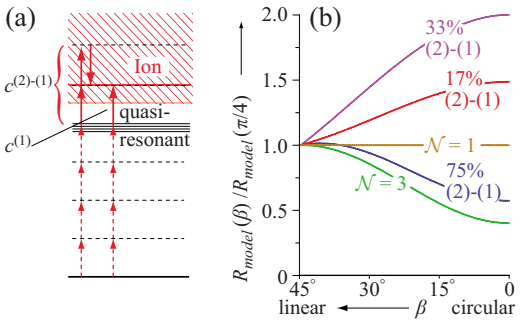

FIG. 5. (Color online) Schematic illustration of interference between different order amplitudes. (a) Hypothetical term scheme for combined action of a three- and a one-photon amplitude ($c^{(2)\text{-}(1)}$ and $c^{(1)}$, respectively) inducing transitions into the ionization continuum from high-lying Rydberg states. (b) Ionization probabilities modeled for the situation shown in (a) with different relative contributions w (%) from $c^{(2)\text{-}(1)}$.

number of steps $\mathcal{N}-\mathcal{K}$ induced by $\hat{P}^+$ ($\Delta m=1$). Summing over all pathways we obtain in accordance with Eq. (26) an overall amplitude

$$c(\mathcal{N},\mathcal{K}) = \binom{\mathcal{N}}{\mathcal{K}} \sin^{\mathcal{K}}\beta \cos^{\mathcal{N}-\mathcal{K}}\beta. \tag{27}$$

Squaring these and summing over all final states leads again to the "classical" result in form (9).

3. Interference of different order processes

So far we have included only absorption processes into our discussion: the energy difference $\hbar\omega_{ba}$ between initial and final states in an $\mathcal{N}$-photon process is matched by $\mathcal{N}\hbar\omega=\hbar\omega_{ba}$. However, for higher intensities (as encountered in our experiments near or above saturation), one may well imagine processes with $\mathcal{N}+2$ photons leading to the same final-state energy, possibly with amplitudes of comparable magnitude. This is illustrated in Fig. 5(a). Assume, e.g., that four photons populate a set of high-lying states quasiresonantly. One additional photon may ionize the system (amplitude $c^{(1)}$), or alternatively the same final continuum state may be addressed by two-photon absorption accompanied by one-photon-stimulated emission (amplitude $c^{(2)\text{-}(1)}$). We may obtain some feeling for the consequences, if such two processes act coherently, by adding the amplitudes of these processes.

We first note that, since stimulated emission is involved as indicated in Fig. 5, the amplitudes $c^{(2)\text{-}(1)}$ and $c^{(1)}$ may have different signs [50]. Now, for this very crude trend analysis it may suffice to identify the amplitudes with those from the "Pascal model" according to Eq. (27) and set $c^{(2)\text{-}(1)} \propto -c(3,\mathcal{K})$ and $c^{(1)} \propto c(1,\mathcal{K})$. Adding these amplitudes with different weights w and summing over the squares gives then a model ionization rate for such processes:

$$R_{model} = \sum_{\mathcal{K}=0}^{3} [c(1,\mathcal{K}) - wc(3,\mathcal{K})]^2. \tag{28}$$

We note that R_{model} is no longer necessarily proportional to a power of the laser intensity and the choice of w is completely arbitrary here. However, as clearly demonstrated by the results shown in Fig. 5(b), interference of the two processes of different orders may—under special circumstances—lead to an increase in the signal for circularly polarized light, in complete contrast to the pure absorption processes which we have treated before (see Fig. 3).

D. Two-photon absorption by two active electrons

In Sec. III C we have exclusively discussed systems with a single active electron (SAE model). While this may be an appropriate first-order approach to the treatment of ionization for many atomic systems, it is certainly not adequate to describe the interaction of the strong field with the 240 valence electrons of C_{60}. Thus we have to pose the question of how the polarization dependence in multiphoton absorption will be modified if more than one electron is excited. To demonstrate the key issues we will concentrate here on the absorption of two photons by two "chromophore" electrons ($k=1$ and 2), each of which absorbs one photon of energy $\hbar\omega$. Thus the total energy deposited into the system is $2\hbar\omega$. For simplicity of the argument, we approximate the electrons as identical two-level systems, their ground and excited states (orbitals) being characterized by $|l_{ak}m_{ak}\rangle$ and $|l_{bk}m_{bk}\rangle$, respectively, with excitation energies $\hbar\omega_{ba}$ for the individual electrons. We neglect any coupling originating from angular momenta or spin, but allow for some radial coupling which will remove the degeneracy of states with only one electron excited. The emerging combined states may then be written [51] as suitably symmetrized and antisymmetrized product states: *ground state* $|l_{a1}m_{a1}l_{a2}m_{a2}\rangle^{\pm,0}$, *singly excited states* $|l_{a1}m_{a1}l_{b2}m_{b2}\rangle^{\pm}$, and *doubly excited states* $|l_{b1}m_{b1}l_{b2}m_{b2}\rangle^{\pm,0}$, with total energies of 0, $\hbar\omega^+$ or $\hbar\omega^-$, and $\hbar\omega^+ + \hbar\omega^-$, respectively. Here the $\pm$ stands for symmetric and antisymmetric combinations of states,

$$|l_{j1}m_{j1}l_{j2}m_{j2}\rangle^{\pm} = \frac{|l_{j1}m_{j1}l_{j2}m_{j2}\rangle \pm |l_{j2}m_{j2}l_{j1}m_{j1}\rangle}{\sqrt{2}}, \tag{29}$$

where the pairs of quantum numbers $(l_{j1}m_{j1})$ and $(l_{j2}m_{j2})$ differ in at least one of l or m, while

$$|l_{j1}m_{j1}l_{j2}m_{j2}\rangle^{0} = |l_jm_jl_jm_j\rangle \tag{30}$$

describes states of + symmetry where both electrons have fully identical angular momentum quantum numbers.

In order to evaluate Eq. (20) explicitly for the case at hand, we have to rewrite the dipole operator in Eq. (13) as

$$\vec{D}\cdot\vec{e} = e_0\vec{r}_1\cdot\vec{e} + e_0\vec{r}_2\cdot\vec{e} = (e_0\vec{r}_1 + e_0\vec{r}_2)\cdot\vec{e}. \tag{31}$$

However, $\vec{r}_1$ acts only on electron 1 and $\vec{r}_2$ only on electron 2. The relevant products of transition amplitudes in Eq. (20) can thus be written as sums over products,

$$\langle l_{b2}m_{b2}|\hat{P}|l_{a2}m_{a2}\rangle\langle l_{b1}m_{b1}|\hat{P}|l_{a1}m_{a1}\rangle.$$

We also notice that transition matrix elements between states of different symmetries vanish, reducing the number of states involved as intermediates significantly.

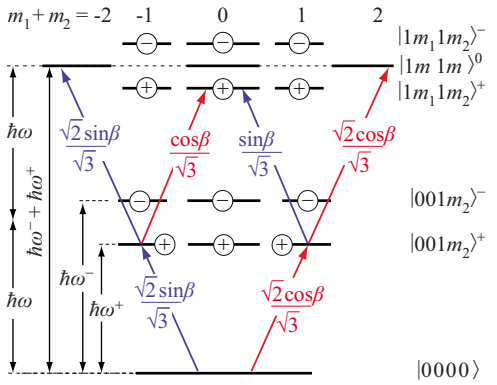

FIG. 6. (Color online) Energy levels and states $|l_1 m_1 l_2 m_2\rangle^{\pm,0}$ of the two combined chromophore electrons with the relevant dipole-allowed transition amplitudes for the LHC and RHC polarized components of the radiation field. (Note that the arrows indicate amplitudes, not energy resonance or population transfer.) All levels with $l_1 \equiv l_2 = 1$ are degenerate; they are drawn, however, as split for clarity.

1. Simple example for two chromophores

Before evaluating Eq. (20) for arbitrary angular momenta, we illustrate by the simplest example how the amplitudes add and how the summation over all intermediate and final states operates in this case. So let us assume that each of the two electrons can have an angular momentum $l_{1,2}=0$ or 1, their product states being $|l_1 m_1 l_2 m_2\rangle^{\pm,0}$. Together with the corresponding energy levels, the dipole transition amplitudes involved are illustrated in Fig. 6.

To verify the values for the transition amplitudes given in Fig. 6, we note that the initial ground state $|0000\rangle$ is symmetric. Hence, with $\Delta m = q = \pm 1$ and using Eq. (14) with Eqs. (17) and (18), only the $|001 \pm 1\rangle^+$ states can be excited in the first step and the transition amplitudes are $\propto \cos\beta/\sqrt{3}$ and $\sin\beta/\sqrt{3}$, for the LHC and RHC polarized components, respectively. From definitions (29) and (30) a factor of $2 \times 1/\sqrt{2} = \sqrt{2}$ enters for these $|\cdots\rangle^0 \to |\cdots\rangle^+$ transitions. The same holds for the next step in case of a $|\cdots\rangle^+ \to |\cdots\rangle^0$ transition. However, for $|\cdots\rangle^+ \to |\cdots\rangle^+$ transitions this factor becomes $2 \times 1/2 = 1$. We can now read the amplitudes for reaching the three relevant final states from Fig. 6 as products of the two single-step amplitudes ($\times 2$ for the $|111-1\rangle^+$ state which can be reached by two different pathways). The two-photon-absorption cross section is then proportional to the sum of amplitudes squared:

$$\sigma^{(2)} \propto \left(\frac{2}{3}\cos\beta\cos\beta\right)^2 + \left(\frac{2}{3}\sin\beta\sin\beta\right)^2 + \left(2\frac{\sqrt{2}}{3}\sin\beta\cos\beta\right)^2 = \frac{4}{9}.$$

Thus, the two-photon-absorption cross section by two chromophores becomes *independent* of the circular polarization angle β. This is indeed an important finding: the polarization dependence behaves like two one-photon absorption acts of two independent electrons—although the two electrons interact with each other in the intermediate state so that their wave functions have to be properly symmetrized (or antisymmetrized) and their energy levels split. However, the overall probability, i.e., the rate for the process according to Eq. (2), is still determined by the fact that two photons are absorbed: the product of two linear absorption processes is $\propto I_0 I_0 = I_0^2$ as for any two-photon process, just as in the SAE case.

2. General case

These considerations can also be applied for arbitrary l_{a1} (l_{b1}) and l_{a2} (l_{b2}). Writing Eq. (20) in the general form

$$\sigma_{ba}^{(2)} \propto \sum_{l_{b1} m_{b1} m_{a1}} \sum_{l_{b2} m_{b2} m_{a2}} |\langle l_{b2} m_{b2}|\hat{P}|l_{a2} m_{a2}\rangle\langle l_{b1} m_{b1}|\hat{P}|l_{a1} m_{a1}\rangle|^2, \tag{32}$$

one obtains after some trivial algebraic reordering

$$\sigma_{ba}^{(2)} \propto \left(\sum_{l_{b1} m_{b1} m_{a1}} |\langle l_{b1} m_{b1}|\hat{P}|l_{a1} m_{a1}\rangle|^2\right) \times \left(\sum_{l_{b2} m_{b2} m_{a2}} |\langle l_{b2} m_{b2}|\hat{P}|l_{a2} m_{a2}\rangle|^2\right), \tag{33}$$

which is simply the product of the two single-photon-absorption cross sections for the two chromophores. As demonstrated in Sec. III C 1, they do not depend on light polarization.

This may be further generalized to the simultaneous excitation of $\mathcal{N}$ chromophores, each absorbing one single photon. Consequently, the *overall* generalized $\mathcal{N}$-photon-absorption cross section is $\propto I_0^{\mathcal{N}}$ but is *not* influenced by the polarization.

3. Double ionization in multiphoton processes

The strategy leading to expression (33) can be generalized to the absorption of $\mathcal{N}_1$ photons by a first electron and $\mathcal{N}_2$ photons by a second one. This will, in principle, e.g., be relevant for double ionization. Here multiphoton absorption by the first active outer-shell electron leads to a singly charged cation, while multiphoton excitation of an additional electron contributing to the cation configuration produces a doubly charged ion. In the spirit of the previous argument the double-ionization cross section will then become

$$\sigma^{(\mathcal{N}_1,\mathcal{N}_2)}(\beta) \propto \sigma^{(\mathcal{N}_1)}(\beta) \times \sigma^{(\mathcal{N}_2)}(\beta). \tag{34}$$

It is important to note that the above argument for deriving this type of polarization dependence during a photon-absorption process of the order $\mathcal{N}_1+\mathcal{N}_2$ appears not to depend on whether the double ionization occurs in one direct double-ionization event (both electrons interact with the field more or less at the same time) or by sequential ionization (where a certain time may elapse between absorptions of the first $\mathcal{N}_1$ and the second $\mathcal{N}_2$ photons). However, the argument used in deriving Eq. (33) will not be valid if the two electrons are strongly correlated in the final state—as, e.g., in doubly excited autoionizing states. Without proof we expect in such a case SAE characteristics to dominate. Consequently the ionization rate will depend on $\sigma^{(\mathcal{N}_1+\mathcal{N}_2)}(\beta)$ rather than on $\sigma^{(\mathcal{N}_1,\mathcal{N}_2)}(\beta)$.

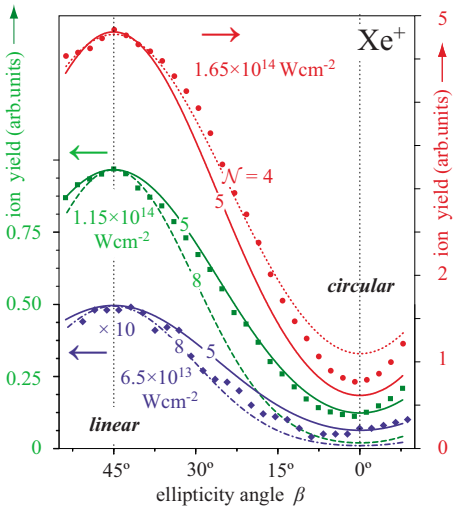

FIG. 7. (Color online) Yield of Xe^+ ions for different intensities as a function of the ellipticity angle β. The signals can be compared to each other (right scale for $I_0=1.65\times10^{14}$ W cm^{-2} and left scale for 1.15×10^{14} and 0.65×10^{14} W cm^{-2}; the latter signal is plotted $\times10$). The smooth lines represent theoretical model (10) with $\mathcal{N}$ given at the curves. The maximum has been normalized to linear polarization ($\beta=\pi/4$).

In general, the two cross sections differ. Nevertheless, quantitative evaluation for $\mathcal{N}_1,\mathcal{N}_2\geq4$ shows that these differences are rather small. For double ionization of Xe where $\mathcal{N}_1=14$ and $\mathcal{N}_2=8$, they become completely negligible. In summary, polarization dependence probes a rather different quality of ionization processes compared to the dependence on laser intensity which is usually reported in the literature.

E. Comparison of experiment and theory for Xe

We now come back to our experimental observations on multiphoton ionization of the Xe atom and compare these results with our theoretical predictions. For a very careful study of the overall Xe^+ and Xe^{2+} ion yields as functions of laser intensity, we refer to [36,37], where the experimental data were compared to various theoretical models. Without going into the specificities, we note that with an ionization potential of 12.129 eV at least eight photons are needed to generate the lowest ionic state $Xe^+(^2P_{3/2})$, but a number of intermediate resonances obscure the expected power law (2) somewhat. Thus, the log-log plot of ion yield vs intensity (see Fig. 1 of [37]) shows a slope of 8 only for intensities below 10^{13} W cm^{-2}, while between 3×10^{13} W cm^{-2} and saturation intensity $I_{0,s}\simeq10^{14}$ W cm^{-2}, a slope of 5 is observed, giving evidence of an effective five-photon process. In Fig. 7 our measured Xe^+ ion yield as a function of the ellipticity angle β is compared to theoretical model (8) for laser intensities of 0.65, 1.15, and 1.65×10^{14} W cm^{-2}, which have been chosen significantly below, just around and somewhat above saturation intensity for Xe^+ ion formation. Obviously, at and below $I_{0,s}$ the assumption of a single-active-electron model with a five-photon process fits the measured results best, while (considering the moderate statistics) we cannot exclude an eight-photon process at the lowest intensity. As one would expect, above saturation the fit with the $\mathcal{N}=5$ polarization dependence becomes less and less convincing, since saturation and geometric effects mimic a lower-order process. Below that region, however, the agreement between experiment and theory is surprisingly good.

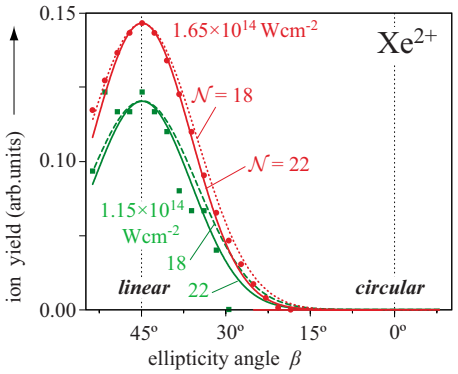

FIG. 8. (Color online) Yield of Xe^{2+} ions as a function of the ellipticity angle β. Scales only on the left; the signal for 1.15×10^{14} W cm^{-2} is plotted $\times10$. Otherwise same as Fig. 7.

This statement holds *a fortiori* for the Xe^{2+} ion yield as a function of β shown in Fig. 8 for laser-pulse intensities of 1.15 and 1.65×10^{14} W cm^{-2}. At least 14 additional photons are needed to generate the lowest $Xe^{2+}(^3P_2)$ ionic state. Our experimental data are compared with model (8) for multiphoton ionization (MPI) processes with $\mathcal{N}=22$ or 18 photons. Within the statistical errors both curves compare reasonably well with the experiment—reflecting the fact that generation of doubly charged Xe^{2+} requires a multiphoton process of the order 8+14 (or 5+14, considering what has been found for Xe^+ formation). Alternatively, we could compare our polarization data to a two-chromophore or sequential process with $\mathcal{N}_1=8$ or 5 and $\mathcal{N}_2=14$ according to Eq. (34). It turns out, however, that the two fit functions are almost identical in this case (within the linewidth of the curves shown in Fig. 8), so that we cannot glean additional information from such a more sophisticated comparison. It is interesting to note, however, that the log-log plots of ion yield v. intensity (see Fig. 3 of [36]) does never show a slope of 22, except perhaps for the lowest intensities of $\sim1.23\times10^{13}$ W cm^{-2}, which still lead to a measurable signal. At intensities of our present polarization study, the log-log data for Xe^{2+} of [36] taken with linear polarization are already flattened substantially due to saturation. In that sense, the polarization-dependent studies probe in a much more sensitive manner the order of the photon-absorption process than mere ion yield measurements. We will make use of this very fact in the following discussion of the data for C_{60} ionization and fragmentation.

In summary, we find a truly astonishing agreement between our model and the experimental observations for MPI of Xe as a test case. In view of the crude assumptions which have entered into the quantum-mechanical justification of classical intensity averaging model (8), this constitutes somewhat of a puzzle, recalling that we ignore differences in resonance denominators and assume l independence of radial matrix elements. We may argue that the rather intense field

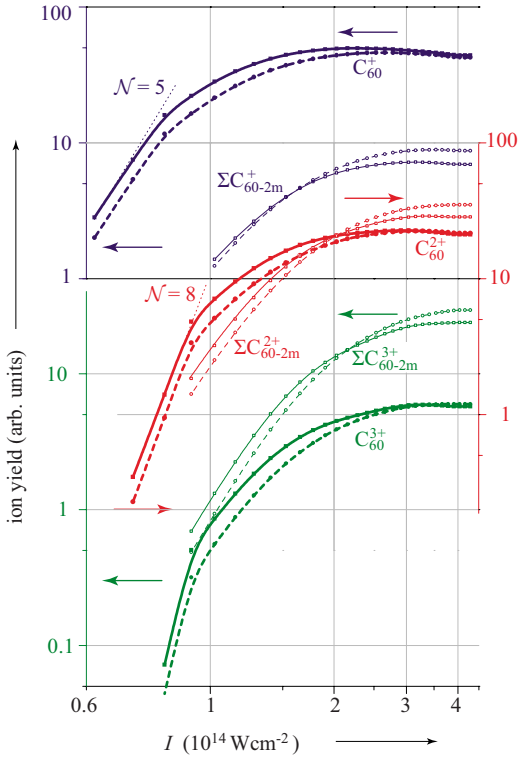

FIG. 9. (Color online) Double-logarithmic plot of ion yields as functions of laser pulse intensity I_0 at 797 nm. The lines shown are spline fits to the experimental data points. Heavy lines (filled data points) and thin lines (empty data points) refer to "parent" and fragment ions, respectively. ■ and □ (full lines) have been measured with linearly polarized light; ● and ○ (dashed lines), with circularly polarized light. The scales for all data are the same but have been shifted with respect to each other for clarity.

used in the present study and the large number of photons (in the spirit of Ref. [41]) involved in the Xe case (in particular for double ionization) create the conditions for the applicability of our approximation. Note that the ponderomotive shift is substantial; e.g., for $I_0=1.15\times10^{14}$ W cm^{-2} we have $U_P=6.8$ eV at 797 nm. Thus, the levels constituting resonance denominators will be shifted—more precisely they will be completely smeared out—and the assumption of *one* representative intermediate level appears to be a reasonable compromise. This would be consistent with Eq. (24). Also, different l states will couple so that the independence of radial matrix elements on l is no longer an issue. In any case, quantitative predictions for ionization rates in elliptically polarized light under these conditions continue to be a substantial challenge for any more accurate theory.

IV. RESULTS AND DISCUSSION FOR C_{60}

Figure 9 gives an overview of all ion yields of charge states $q=1-3$ as functions of laser intensity in the standard log-log plot. The curves shown represent integrations over the mass peaks illustrated in Fig. 1. The fragment signals given for each charge state are summed over the ion yield for all observed fragmentation channels of fullerenelike large fragments C_{60-2m}^{q+}, including the respective metastable fragments. The signals for individual fragments show similar trends.

For linear polarization such data have been reported and discussed in detail over several orders of magnitude in intensity in previous publications (see, e.g., [18,52]). Here we focus on the differences between linear and circular polarizations in an intensity range from slightly below to just above the saturation regime. The well-known multiphoton slopes at lower intensities according to Eq. (2) are indicated by $\mathcal{N}=5$ and 8 for C_{60}^{+} and C_{60}^{2+}, respectively. We recognize pronounced differences for interaction with linearly and circularly polarized light (even though a log-log plot does not emphasize such differences). At low intensities, the observed ion yield is less for all parent and fullerenelike fragment ions, as expected after the detailed discussion in Sec. III. In contrast, at higher intensities the fragment signals become larger for circular polarization than for linear polarization. This is a big surprise, since both the general considerations about polarization dependence given above and the general experience with recolliding electrons would predict the opposite.

Note also that for the signals from not fragmented C_{60}^{q+} the difference between linearly and circularly polarized light disappears for high intensities where saturation is reached. This is what one would expect since saturation in such studies typically occurs when either the parent species is depleted due to the process studied or the observed species is in turn depleted by a subsequent process. Any further increase in the signal is then due to geometry, i.e., due to a continuously increased ionization region in the wings of the Gaussian laser beam. Direct multiphoton ionization of C_{60} leading to not fragmented C_{60}^{q+} fullerenes is thus seen to simply depend on the cycle-averaged power of the laser intensity—which reaches the saturation limit somewhat earlier in the linear case. Specifically, the C_{60}^{+} and C_{60}^{2+} signals even decrease for intensities larger than 2.3×10^{14} W cm^{-2}, mirroring the enhanced fragmentation. The continuing increase in fragment ion signals with intensity for circular polarization with only moderate signs of saturation thus warrants special discussion.

To follow the trends in more detail, Figs. 10–12 present relative ion yields as functions of ellipticity angle β and laser intensity I_0 (797 nm, 27 fs). All data have been normalized to the respective ion yield for linear polarization ($\beta=\pi/4$) to show the crucial observations more clearly. These data have been extracted from the corresponding mass spectra as shown in Fig. 1 for charge states $q=1-3$. Similar data are obtained for $q=4$. There, however, a background from smaller fragments with $q=3$ may slightly obscure the evaluation so that we refrain here from presenting these results.

For each charge state the "parent" ion yield for C_{60}^{q+} is shown in the upper panels, while the lower panels present the sum over all fullerenelike fragment signals $\Sigma_{m\geq1}C_{60-2m}^{q+}$ of a given charge state q. We set "parent" in quotation marks to indicate that in general different microcanonical ensembles are represented by parents and fullerenelike fragments of the same charge which have experienced different histories of ionization and energy deposition. Fragments typically arise from ions which have absorbed many photons and were thus particularly hot directly after the laser pulse. An important

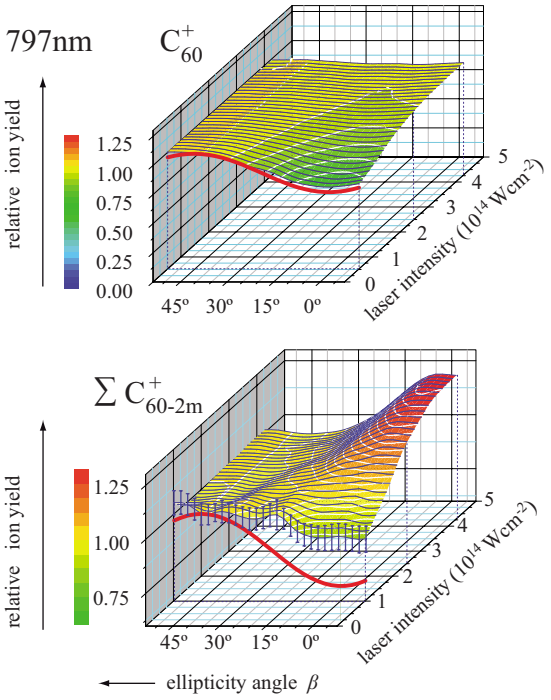

FIG. 10. (Color online) Normalized ion yield as a function of ellipticity angle β and laser intensity I_0 for 797 nm pulses. Top: C_{60}^{+} parent ion; the full (red) line at the lowest intensity represents our model cross section (12) for a two-photon, one-chromophore transition. Bottom: ion yields of fragments C_{60-2m}^{+} summed over all observed channels m after m units of C_2 have been evaporated. Note the different vertical scales. Since the fragment yield is very small at low intensities, we have indicated error bars.

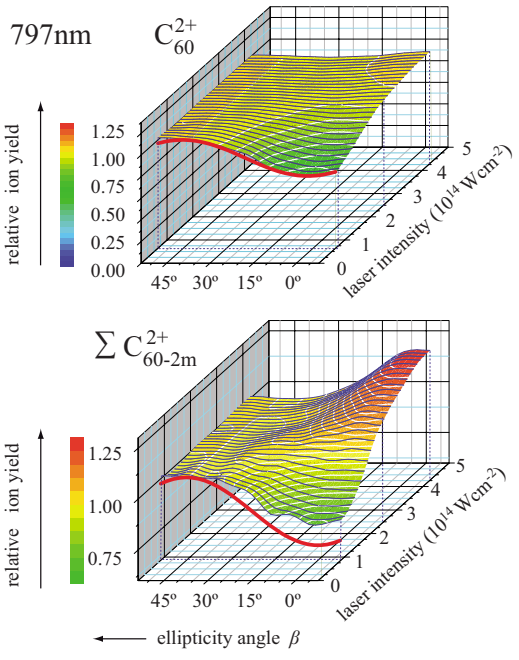

FIG. 11. (Color online) Normalized ion yield as a function of β and laser intensity for 797 nm pulses. Top: C_{60}^{2+} parent ion; bottom: fragments ΣC_{60-2m}^{2+}. Otherwise same as Fig. 10.

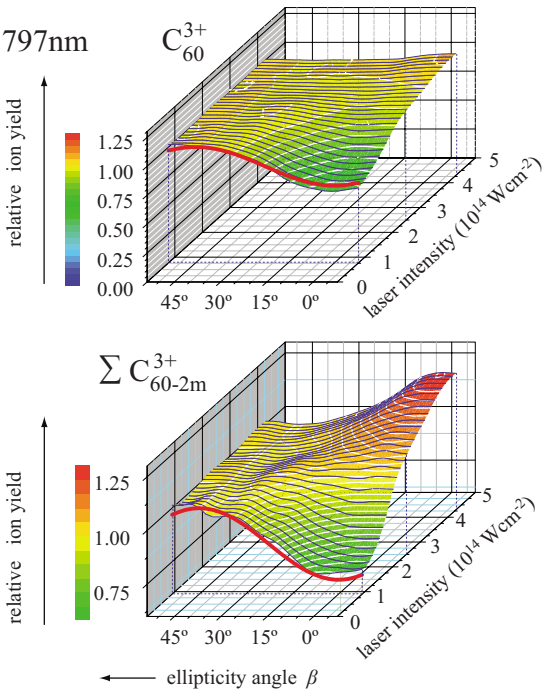

FIG. 12. (Color online) Normalized ion yield as a function of ellipticity angle β and laser pulse intensity I_0 for 797 nm pulses. Top: C_{60}^{3+} parent ion; bottom: fragments ΣC_{60-2m}^{3+}. Otherwise same as Fig. 10.

part of the cooling process is then consecutive evaporation of C_2 molecules. Also, for the higher-charge states we cannot completely rule out some minor contributions from fission processes to fragment formation as observed, e.g., in collisional induced ionization and fragmentation studies [53].

In all cases a small, but very clear reduction in the signal for circularly polarized light is seen at low intensities (0.9×10^{14} W cm^{-2}). Here the ponderomotive potential is only $\simeq 5$ eV and we do not expect recolliding electrons to play a dominant role. However, a nearly perfect match of the observed (low-intensity) β dependence is found with an average intensity distribution $\langle I_0^2(t,\beta)\rangle$ for a *single-electron, two-photon* absorption process according to Eq. (12) as indicated by the full (red) line. This remarkable result manifests the importance of the t_{1g} doorway state (excitation energy $\simeq 3$ eV) related to the t_{1g} orbital, which can be populated by such a coherent two-photon excitation as, e.g., shown by the calculations of Bauer *et al.* [22,23]. (They described C_{60} in a spherical basis and related the corresponding resonance to a transition of the outermost π electron from $l=4$ to $l=5$.) At higher intensities the β dependence of the parent ions decreases and for $I_0 > 2 \times 10^{14}$ W cm^{-2} the yields become almost independent of ellipticity. We attribute this to saturation of the ionization process.

However, while saturation for C_{60}^{+}, C_{60}^{2+}, and C_{60}^{3+} is also observed in the absolute ion yield shown in Fig. 9 (see also [18]) between $I_0 \sim 1$ and 2×10^{14} W cm^{-2}, the clear signature of a two-photon process documented in Figs. 10–12 for the parents leaves us with a puzzle: at this wavelength, pulse duration, and intensity range, the ion yield is $\propto I_0^{\mathcal{N}}$ with $\mathcal{N}=5$, 8, and 11 for C_{60}^{+}, C_{60}^{2+}, and C_{60}^{3+}, respectively. Why

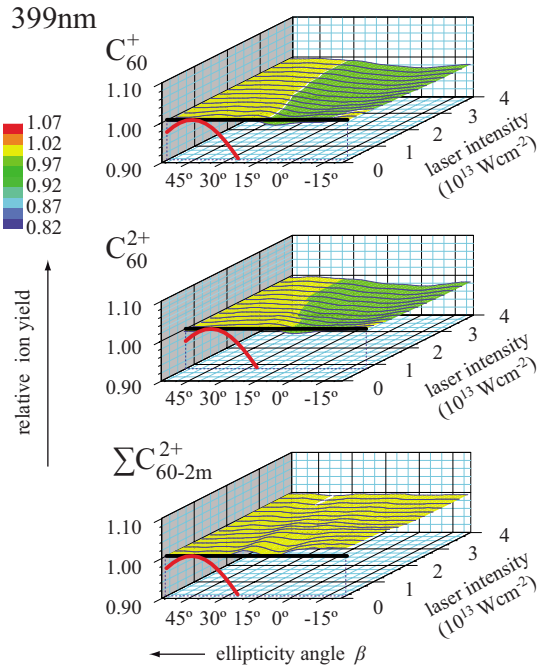

FIG. 13. (Color online) Normalized ion yield as a function of ellipticity angle β and laser pulse intensity I_0 for 399 nm pulses for parent ions C_{60}^{+} and C_{60}^{2+}, and fragments ΣC_{60-2m}^{2+} of parent ions. No change in the yield with ellipticity angle β is observed over the whole intensity range (single-photon absorption; black horizontal line at lowest intensities). Note the magnified vertical scale with respect to Figs. 10–12. For comparison, the two-photon, one-chromophore model (12) is also indicated at lowest intensities in red.

is there no corresponding dependence (see Fig. 3) observed as a function of ellipticity angle β? Even if we distrust the general validity of Eq. (12), the contrast to the Xe^{+} case (Fig. 7) is striking. We consider this strong evidence for genuine multielectron processes (NMED) dominating the ionization and energy deposition in C_{60} as tentatively invoked in our earlier work: once the doorway state is reached, many electrons can absorb energy through transitions in a quasicontinuum of states, which in fact explains the high number of photons absorbed. As we have explicitly shown (for the case of $\mathcal{N}=2$) in Fig. 3, one expects no polarization dependence if each of the $\mathcal{N}$ more or less loosely coupled chromophore electrons absorbs one photon, while the overall intensity dependence is still determined by Eq. (2). For a process which requires an energy equivalent of at least five photons, such as C_{60}^{+} formation, the intensity dependence will thus be $\propto I_0^5$ since five photons must be absorbed during the laser pulse by a single C_{60} and the corresponding statements hold for higher-charge states.

As a crucial test we have also measured the ellipticity dependence of the C_{60}^{q+} and C_{60-2m}^{q+} signals at $\lambda = 399$ nm for intensities $I_0 \sim (0.2-3.9) \times 10^{13}$ W cm^{-2}. Figure 13 gives some examples, documenting that the 3D plots of the relative ion yield all are absolutely flat to within $\simeq 1\%$. In contrast, we know from earlier work that the ion yields as functions of intensity at this wavelength are $\propto I_0^3$ and $\propto I_0^4$ for C_{60}^{+} and C_{60}^{2+}, respectively [12], with a saturation intensity just below 1×10^{14} W cm^{-2} for C_{60}^{+}. This strongly confirms the key role of the doorway state, being excited by absorption of a single 399 nm photon so that its population depends only on I_0 and not on β. Again, subsequent photons are deposited via different chromophore electrons, of which each absorbs one photon.

Returning to 797 nm, the ion yields of fullerenelike fragments C_{60-2m}^{q+} are even more surprising, as seen in the lower parts of Figs. 10–12. While at lower intensities one still sees a β dependence which may be taken as signature for a two-photon process—at least for C_{60-2m}^{3+}—for C_{60-2m}^{+} fragments very weak and noisy signal does not allow a clear conclusion, and the C_{60-2m}^{2+} fragment yield is somewhat intermediate. However, at higher intensities a significant enhancement of the fragment signal is observed with circularly polarized light. At first sight, this appears to be against all common wisdom: typically fragment signals decrease with circularly polarized light. One potential explanation could be the combination of different amplitudes for different types of multiphoton processes with absorption and induced emission steps leading to constructive interference as indicated in Fig. 5(b). In view of the fact that at high intensities a multitude of intermediate states could play a role, in particular the intense giant resonance between the first ionization threshold and about 35 eV. This is just pure speculation and the question is of course why this should be specific to generate fragments rather than higher-charge states.

Thus, we come back to the potential influence of rescattered electrons mentioned in Sec. I. We first note that the quivering amplitude of a free electron in the field of an 800 nm laser pulse at $I_0 = 10^{14}$ W cm^{-2} is 0.83 nm only, about twice the size of the C_{60} shell radius (0.43 nm [54]). Thus, in contrast to point sources where one expects recollision only for linearly polarized light, one may well imagine loops of recolliding electrons in a circularly polarized electric field interacting with an extended object such as C_{60}—especially so if the electrons ejected have initial kinetic energy (see, e.g., [35], and our own preliminary results [28]). Rescattering for extended atomic systems has recently also been discussed in the context of Xe- and Ar-cluster ionizations [55]. Electrons may indeed be ejected with relatively high initial kinetic energy due to strong-field absorption of many photons. If, e.g., the C_{60} plasmon resonance supports the photoabsorption process in the continuum [18], one expects initial kinetic energies of up to 30 eV. Assuming the electrons to be ejected radially, this will lead most trajectories in a linearly polarized field to miss the C_{60} on return. In contrast, one may find a number of trajectories in a circularly polarized field which return, even several times, as exemplified in Fig. 14 for a few specific initial parameters.

For the present classical trajectory studies we have employed a commonly used model potential (see, e.g., [56]) for the C_{60}^{q+} ions, parametrized similarly to our previous work [18], including polarization screening [24] adopted in such a way that the field is zero inside. Details are described in the Appendix. Experiments together with such trajectory studies documented that at long wavelengths (1500 nm), fragmentation is significantly amplified by recollision in linearly polarized laser fields [25]. With the present 3D trajectory calculations we find at correspondingly lower ponderomotive

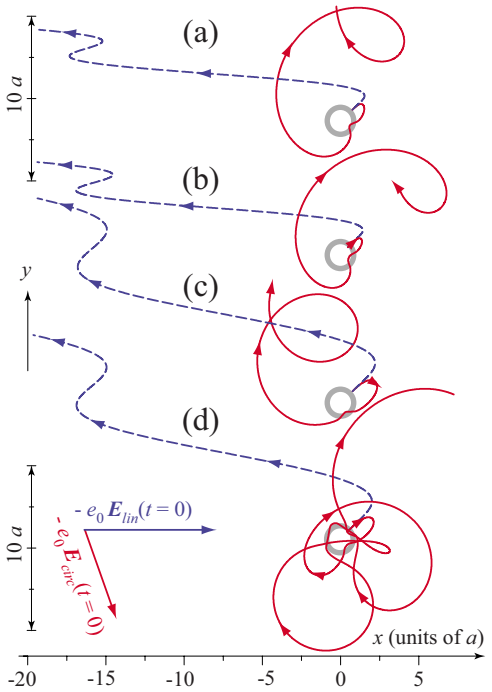

FIG. 14. (Color online) Examples of classical electron trajectories in the combined field of C_{60}^{+} and linearly (dashed lines) or circularly (full lines) polarized light. $I_0=4.3\times10^{14}$ W cm^{-2}, 797 nm, initial kinetic energy is [(a) and (b)] 1 eV or [(c) and (d)] 10 eV, and starting point of the trajectory is [(b) and (d)] $0.65a$ or [(a) and (c)] $1a$. The initial field phase at $t=0$ is $\varphi=162°$ in all cases shown, implying that the force on the electron at $t=0$ points into the direction of $-72°$ for circularly polarized light and into $+x$ direction as indicated by the vectors. All distances are given in units of the C_{60} radius a. The thick gray full circles indicate the C_{60} shell with the thickness of $0.35a$.

potentials at 800 nm the opposite: electron trajectories in a circularly polarized field starting at the C_{60} radius a or at the inner-shell radius $b=0.65a$ (with or without initial kinetic energy) return significantly more often. As an example, the recollision probabilities derived from such trajectory studies at high laser intensity (with initial kinetic energy) are shown in Fig. 15. As clearly seen, the recollision probability in circularly polarized light exceeds that for linear polarization—if the electrons were assumed to be born with energies of up to 10 eV). About 15% of the trajectories return in circularly polarized light, while only 11% recollide for linear polarization. On the other hand, there are still a small, but nonnegligible number of trajectories in linearly polarized light, which return with much higher energies—up to the well-known value of $3.17U_P$ as indicated in Fig. 15—while trajectories in circularly polarized light only harvest up to 25 eV. At lower laser intensities this limit decreases as one would expect.

It should be pointed out that this trajectory study is not intended to give a quantitative or even qualitative explanation for the experimentally observed enhancement of fragments created by circularly polarized light over those excited by linearly polarized light at high laser intensities. This cannot be expected from a single-electron trajectory study in a situation which we have shown to be dominated by multi-

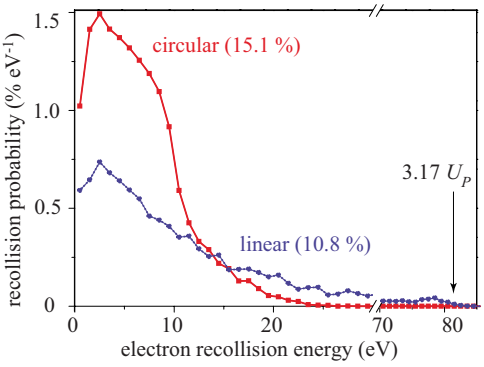

FIG. 15. (Color online) Probabilities of finding different recollision energies for electrons emitted from the inner (b) and outer radii (a) of the C_{60} molecule in linearly or circularly polarized light at $I_0=4.3\times10^{14}$ W cm^{-2}, 797 nm. Initial conditions are taken statistically: kinetic energies of 0–10 eV (radial emission) at $0\leq\Phi<2\pi$, laser field phase (at $t=0$) $0\leq\varphi<2\pi$, and starting radius of $0.65a$ or a.

electron dynamics. Our key point here is just to illustrate that the general belief about circular polarization being unable to lead to energy deposition due to recollision is not necessarily true for extended systems and strong laser fields. A more sophisticated calculation in the spirit of those done for rare-gas clusters [57] may lead to interesting results when the ionizing field is circular rather than linear. In view of the example trajectories shown in Fig. 14, one may very well imagine a vehement collective motion and collisions in a many-electron system driven by elliptically polarized strong laser fields. This certainly could lead to substantial heating of the electron gas and subsequently of the nuclear backbone—which is then finally probed by fragmentation long after the laser pulse is over.

V. SUMMARY

In summary, the present work has shown that understanding the ionization dynamics in strong pulsed laser fields may profit significantly from studies with elliptically polarized light, both in atoms and in large finite systems. As a first test case we have seen that the ion yields of Xe^{+} and Xe^{2+} decrease dramatically when the typical linear polarization of the ionizing light pulse was changed to elliptic and finally circular polarization. It turned out in this case that the exact dependence on the ellipticity angle β follows surprisingly well the cycle-averaged $\mathcal{N}$th power of the time-dependent intensity, where $\mathcal{N}$ is the number of photons absorbed. We have derived a hand-waving quantum-mechanical interpretation of this behavior, which is inspired by strong-field approximations (SFAs).

Further analysis also shows that such studies of the dependence on β allow one in principle to distinguish between SAE mechanisms in the ionization process and multielectron dynamics (NMED): the total ion yield below saturation rises in both cases typically with the $\mathcal{N}$th power of the intensity. Thus from a log-log plot of ion yield vs laser intensity, one obtains in the usual way an estimate of the critical number of

photons involved. However, ellipticity dependence is only observed when SAE processes play a key role: a significant drop in ion yield with increasing ellipticity is predicted and observed. The higher is the number $\mathcal{N}$ of photons absorbed, the more dramatic this drop turns out to be. In contrast, no ellipticity dependence is expected when many electrons (chromophores) are independently excited. This opens up hitherto unexplored pathways for studying energy deposition and ionization dynamics in strong pulsed laser fields for clusters and other large finite systems, but possibly also for atoms and molecules.

As a historical side remark we note that in the early days of multiphoton processes (i.e., in the 1970s), studies with elliptically and circularly polarized light were soon disregarded when it became clear that the ionization probabilities in general decrease dramatically in comparison to linearly polarized light. Today, with strong laser fields readily available, one may recognize elliptically polarized light as a very special tool and a challenge for gleaning novel insights into laser-matter interaction.

Our present studies of C_{60} fullerene ionization and fragmentation dynamics present an example of such understanding. We have observed a significant influence of ellipticity on ionization and fragmentation processes in C_{60} in moderately intense femtosecond laser pulses at 797 nm. The decrease in ion yields at lower intensities gives strong evidence of the crucial role of the t_{1g} state as a doorway state for energy deposition, followed by efficient multielectron dynamics. This is corroborated by corresponding studies with 399 nm pulses, where no such dependence is observed since the doorway state can already be reached with one photon only. Interestingly, no higher-order polarization dependence is seen in the ion yield for all observed C_{60}^{q+} charge states, although at least five photons of 797 nm are needed to generate C_{60}^{+} and an additional eight for detecting C_{60}^{2+}. This is a clear indication that multielectron dynamics takes over as soon as the doorway state has been reached. At even higher intensities the parent C_{60}^{q+} ion signals do not depend on β at all due to saturation and geometrical effects.

In contrast, for 797 nm and intensities above 10^{14} W cm^{-2} a remarkable increase in fullerenelike fragments C_{60-2m}^{q+} is observed in circularly polarized light, giving evidence of higher-energy deposition by circularly polarized laser fields. Obviously, recolliding electron trajectories due to linearly polarized light which are often held responsible for enhanced fragmentation do not play a dominant role in the presently observed process. In the contrary, classical trajectory studies suggest that due to the particular structure of C_{60} semiclosed loops of recolliding electrons may occur in circularly polarized light. Surprisingly, the electron recollision probability may even be higher for circularly than for linearly polarized light.

Although we have at present no conclusive interpretation for the observed enhanced heating, we suggest that a more rigorous study of the electron dynamics in elliptically polarized fields may turn out to be a very promising challenge for theory. One might envisage quasiclassical models, as successfully employed in rare-gas clusters, as well as in-depth time dependent density functional theory (TDDFT) approaches incorporating elliptic polarization. On the experimental side, electron spectra from the processes, observed at present by ion yield, are expected to be very informative, in particular when measured in coincidence with the ions. Such work is in progress in our laboratory.

Note added in proof. Recently, Reiss [59] pointed out to us that in strong field ionization of a single electron by circularly polarized light, conservation of angular momentum requires the electron to escape tangentially from the atom—in contrast to our assumption of radial ejection. However, in the present case we can safely assume that due to the multielectron nature of the ionization process substantial energy and angular momentum will be exchanged among the valence electrons. Thus, radial emission of electrons with significant kinetic energy is one of many possible choices for initial conditions in the multielectron case.

ACKNOWLEDGMENTS

We thank H. R. Reiss for stimulating discussions. This work was supported by the German Research Foundation (DFG) via the collaborative research centre 450, "Analysis and Control of Ultrafast Photoinduced Reactions," project A2.

APPENDIX: RECOLLISION TRAJECTORY STUDIES FOR C_{60}

We consider the free-electron motion under the influence of an external laser field and an effective potential of the C_{60} core. Using classical mechanics to describe the electron motion $\vec{r}(t)$, one can write with m_e as the electron mass and e_0 as the electron charge the following:

$$\ddot{\vec{r}}(t) = \frac{\vec{r}}{r}\frac{F(r)}{m_e} - \frac{e_0\vec{E}(t)}{m_e}s(\rho). \tag{A1}$$

The force $F(r)=-e_0 dV(r)/dr$ by which the C_{60} core acts on the electron (charge e_0, mass m_e) is derived from a model potential $V(r)$ very similar to that previously employed [18,58]. It describes C_{60}^{+} essentially as a potential well with outer and inner radii of $a=4.29\times10^{-10}$ m and $b=0.65a$, respectively, approaching asymptotically a Z/r Coulomb potential for $r\gg a$. For the present classical trajectory calculations we have approximated the model in its most recent form [56], smoothing, however, the very sharp (and physically unrealistic) edges over a width of $w=0.15$ by sigmoid functions, while the potential depth was adjusted for $Z=1$ and 2 to $V_0=1.633$ and 1.769 so that the binding energy of the additional electron corresponds to the experimental values of −7.56 and −11.8 eV, respectively. Explicitly our model potential reads (here V, r, and all parameters are in a.u.)

$$V(r;Z) = -\frac{q_a e^{(a-r)/w_1}+Z}{r}\frac{1}{1+e^{(a-r)/w}} - \left(V_0+\frac{Z-1}{a+b}\right) \times\left(\frac{1}{1+e^{(r-a)/w}}+\frac{1}{1+e^{(b-r)/w}}-1\right) - \frac{q_i e^{(r-b)/w_1}+q_0}{a}\frac{1}{1+e^{(r-b)/w}}, \tag{A2}$$

with $w_1=1.59$, $q_a=4.5$, $q_i=2.68$, and $q_0=0.73$. From this we obtain a smooth force function well suitable for the integration procedure. $\vec{E}(t)$ is the electric field of the laser radiation according to Eq. (6), which reads

$$E_x = -E_0 \sin(\beta+\pi/4)\sin(\omega t+\varphi),$$

$$E_y = -E_0 \cos(\beta+\pi/4)\cos(\omega t+\varphi),$$

$$E_z = 0$$

in Cartesian coordinates with the field amplitude $E_0=\sqrt{2Z_0I_0}$, the laser frequency ω, a free initial phase parameter φ, and the ellipticity angle β. The function $s(\rho)$ describes polarization screening of the laser field outside the C_{60} in the spirit of [24] and in addition full screening of the field inside the C_{60} core ($r<0.65a$). For simplicity we use again a sigmoid function which serves this purpose sufficiently well:

$$s(\rho) = \frac{1}{1+e^{(1.5a-\rho)/0.4a}}. \tag{A3}$$

With $\rho=\sqrt{x^2(t)+y^2(t)}$ (assuming the electric field vector to lie in the xy plane) and $r=\sqrt{x^2(t)+y^2(t)+z^2(t)}$, we rewrite Eq. (A1) as

$$\ddot{x}(t) = \frac{s(\rho)e_0E_0}{m_e}\sin\left(\beta+\frac{\pi}{4}\right)\sin(\omega t+\varphi)+\frac{x}{r}\frac{F(r)}{m_e},$$

$$\ddot{y}(t) = \frac{s(\rho)e_0E_0}{m_e}\cos\left(\beta+\frac{\pi}{4}\right)\cos(\omega t+\varphi)+\frac{y}{r}\frac{F(r)}{m_e},$$

$$\ddot{z}(t) = \frac{z}{r}\frac{F(r)}{m_e}. \tag{A4}$$

We assume the electron to be ejected radially with an initial kinetic energy T_{in} from the C_{60} molecule at a position given by r_0, Θ, and Φ. Thus, initial conditions

$$x(0) = r_0 \sin\Theta\cos\Phi,$$

$$y(0) = r_0 \sin\Theta\sin\Phi,$$

$$z(0) = r_0 \cos\Theta,$$

$$\dot{x}(0) = \sqrt{2T_{in}/m_e}\sin\Theta\cos\Phi,$$

$$\dot{y}(0) = \sqrt{2T_{in}/m_e}\sin\Theta\sin\Phi,$$

$$\dot{z}(0) = \sqrt{2T_{in}/m_e}\cos\Theta \tag{A5}$$

are used and differential equations (A4) are solved with MATHEMATICA to derive $\vec{r}(t)$ as well as the electron kinetic energy $T(t)$.

In the present exploratory study we compute a few trajectories for a selection of initial conditions in detail to illustrate interesting cases for linear ($\beta=\pi/4$) and circular ($\beta=0$) polarizations. In addition we have run several 100 000 trajectories at each intensity for an analysis of recollision energies, using a Monte Carlo approach. For these trajectories the electrons are assumed to be ejected into the continuum with randomly chosen values of the initial total energy from $0\ \text{eV}\le W_{in}\le 10\ \text{eV}$, field phases from $0\le\varphi<2\pi$, at $r_0=a$ or b, and with starting angles from $0\le\Phi\le 2\pi$ and $0.95\pi/2\le\Theta<\pi/2$ (i.e., close to the xy plane where the recollision probability is largest). The total recollision energy W_{rec} was derived from returning trajectories at an arbitrarily chosen distance between $b\le r\le a$ where the electron density of the target is largest. Note that the initial kinetic energy T_{in} as well as the final total energy W_{rec} is derived via $W(t)=T(t)+V(r,Z)$ since the classical trajectories allow only the determination of $T(t)=m_e\dot{r}^2/2$. The latter is of course inside the potential much larger than the accessible recollision energy of the free electron in the continuum. The results discussed in Sec. IV are representative samples. We have also studied different intensities and higher initial kinetic energies, as well as higher-charge states. The trends described in Sec. IV are in line with these further computations. We have also switched off screening function (A3), which led to slightly larger recollision probabilities and energies for both linear and circular polarizations, but no dramatic changes in the overall results were observed.

[1] A. N. Markevitch, D. A. Romanov, S. M. Smith, H. B. Schlegel, M. Y. Ivanov, and R. J. Levis, Phys. Rev. A **69**, 013401 (2004).

[2] S. I. Chu and D. A. Telnov, Phys. Rep. **390**, 1 (2004).

[3] A. N. Markevitch, D. A. Romanov, S. M. Smith, and R. J. Levis, Phys. Rev. A **75**, 053402 (2007).

[4] I. V. Hertel, T. Laarmann, and C. P. Schulz, Adv. At. Mol., Opt. Phys. **50**, 219 (2005).

[5] R. Sahnoun, K. Nakai, Y. Sato, H. Kono, Y. Fujimura, and M. Tanaka, Chem. Phys. Lett. **430**, 167 (2006).

[6] K. Nakai, H. Kono, Y. Sato, N. Niitsu, R. Sahnoun, M. Tanaka, and Y. Fujimura, Chem. Phys. **338**, 127 (2007).

[7] M. Ruggenthaler, S. V. Popruzhenko, and D. Bauer, Phys. Rev. A **78**, 033413 (2008).

[8] A. Jaron-Becker, A. Becker, and F. H. M. Faisal, J. Chem. Phys. **126**, 124310 (2007).

[9] G. P. Zhang and T. F. George, Phys. Rev. B **76**, 085410 (2007).

[10] G. P. Zhang, Int. J. Mod. Phys. B **21**, 5167 (2007).

[11] E. E. B. Campbell, K. Hansen, K. Hoffmann, G. Korn, M. Tchaplyguine, M. Wittmann, and I. V. Hertel, Phys. Rev. Lett. **84**, 2128 (2000).

[12] M. Tchaplyguine, K. Hoffmann, O. Dühr, H. Hohmann, G. Korn, H. Rottke, M. Wittmann, I. V. Hertel, and E. E. B. Campbell, J. Chem. Phys. **112**, 2781 (2000).

[13] E. E. B. Campbell, K. Hoffmann, and I. V. Hertel, Eur. Phys. J.

D **16**, 345 (2001).
[14] F. Lepine and C. Bordas, Phys. Rev. A **69**, 053201 (2004).
[15] M. Boyle, K. Hoffmann, C. P. Schulz, I. V. Hertel, R. D. Levine, and E. E. B. Campbell, Phys. Rev. Lett. **87**, 273401 (2001).
[16] M. Boyle, T. Laarmann, K. Hoffmann, M. Heden, E. E. B. Campbell, C. P. Schulz, and I. V. Hertel, Eur. Phys. J. D **36**, 339 (2005).
[17] T. Laarmann, I. Shchatsinin, A. Stalmashonak, M. Boyle, N. Zhavoronkov, J. Handt, R. Schmidt, C. P. Schulz, and I. V. Hertel, Phys. Rev. Lett. **98**, 058302 (2007).
[18] I. Shchatsinin, T. Laarmann, G. Stibenz, G. Steinmeyer, A. Stalmashonak, N. Zhavoronkov, C. P. Schulz, and I. V. Hertel, J. Chem. Phys. **125**, 194320 (2006).
[19] I. Shchatsinin, T. Laarmann, N. Zhavoronkov, C. P. Schulz, and I. V. Hertel, J. Chem. Phys. **129**, 204308 (2008).
[20] S. A. Trushin, W. Fuss, and W. E. Schmid, J. Phys. B **37**, 3987 (2004).
[21] G. P. Zhang, X. Sun, and T. F. George, Phys. Rev. B **68**, 165410 (2003).
[22] D. Bauer, F. Ceccherini, A. Macchi, and F. Cornolti, Phys. Rev. A **64**, 063203 (2001).
[23] D. Bauer, Habilitation thesis, Technische Universität Darmstadt, 2002.
[24] V. R. Bhardwaj, P. B. Corkum, and D. M. Rayner, Phys. Rev. Lett. **91**, 203004 (2003).
[25] V. R. Bhardwaj, P. B. Corkum, and D. M. Rayner, Phys. Rev. Lett. **93**, 043001 (2004).
[26] L. V. Keldysh, Sov. Phys. JETP **20**, 1307 (1965).
[27] F. A. Rajgara, M. Krishnamurthy, and D. Mathur, Phys. Rev. A **68**, 023407 (2003).
[28] I. V. Hertel, I. Shchatsinin, T. Laarmann, N. Zhavoronkov, H.-H. Ritze, and C. P. Schulz, Phys. Rev. Lett. **102**, 023003 (2009).
[29] P. Dietrich, N. H. Burnett, M. Ivanov, and P. B. Corkum, Phys. Rev. A **50**, R3585 (1994).
[30] A. Flettner, J. König, M. B. Mason, T. Pfeifer, U. Weichmann, R. Düren, and G. Gerber, Eur. Phys. J. D **21**, 115 (2002).
[31] G. D. Gillen, M. A. Walker, and L. D. Van Woerkom, Phys. Rev. A **64**, 043413 (2001).
[32] C. L. Guo, J. Phys. B **38**, L323 (2005).
[33] H. Sakai, J. J. Larsen, I. Wendt-Larsen, J. Olesen, P. B. Corkum, and H. Stapelfeldt, Phys. Rev. A **67**, 063404 (2003).
[34] M. Murakami, M. Tanaka, T. Yatsuhashi, and N. Nakashima, J. Chem. Phys. **126**, 104304 (2007).
[35] N. I. Shvetsov-Shilovski, S. P. Goreslavski, S. V. Popruzhenko, and W. Becker, Phys. Rev. A **77**, 063405 (2008).
[36] S. Larochelle, A. Talebpour, and S. L. Chin, J. Phys. B **31**, 1201 (1998).
[37] S. F. J. Larochelle, A. Talebpour, and S. L. Chin, J. Phys. B **31**, 1215 (1998).
[38] P. Lambropoulos, Phys. Rev. Lett. **28**, 585 (1972).
[39] S. Klarsfeld and A. Maquet, Phys. Rev. Lett. **29**, 79 (1972).
[40] F. H. M. Faisal, J. Phys. B **5**, L233 (1972).
[41] H. R. Reiss, Phys. Rev. Lett. **29**, 1129 (1972).
[42] N. L. Manakov and V. D. Ovsyannikov, Sov. Phys. JETP **52**, 895 (1980).
[43] Y. Liang, M. V. Ammosov, and S. L. Chin, J. Phys. B **27**, 1269 (1994).
[44] H. R. Reiss, Phys. Rev. A **22**, 1786 (1980).
[45] I. V. Hertel and C. P. Schulz, *Atome, Moleküle und Optische Physik* (Springer, Berlin, 2008), Vol. 1.
[46] I. Gradsteyn and I. Ryzhik, *Tables of Integrals, Series, and Products* (Academic, New York, 1980).
[47] H. R. Reiss, Phys. Rev. A **42**, 1476 (1990).
[48] This essentially amounts to assuming that the strong laser field fully smears out all relevant intermediate energy levels.
[49] D. Brink and G. Satchler, *Angular Momentum*, 3rd ed. (Oxford University Press, Oxford, 1994).
[50] This may most easily be seen in a perturbation approach, where the probability amplitude for absorption is derived by integrating over the $\exp(-i\omega t)$ term of field amplitude (6), while stimulated emission originates from integrating over $\exp(i\omega t)$ and has, consequently, the opposite sign.
[51] Formally, one might also write these states as properly coupled states $|(l_1 l_2)LM\rangle$ with total angular momentum L. However, since no specific angular momentum coupling potential is active, this would only lead to trivial complications in the evaluation of transition matrix elements without changing the final result.
[52] E. E. B. Campbell, K. Hoffmann, H. Rottke, and I. V. Hertel, J. Chem. Phys. **114**, 1716 (2001).
[53] A. Reinkoster, B. Siegmann, U. Werner, and H. O. Lutz, Radiat. Phys. Chem. **68**, 263 (2003).
[54] M. S. Dresselhaus, G. Dresselhaus, and P. C. Eklund, *Science of Fullerenes and Carbon Nanotubes* (Academic, San Diego, 1996).
[55] U. Saalmann and J. M. Rost, Phys. Rev. Lett. **100**, 133006 (2008).
[56] M. E. Madjet, H. S. Chakraborty, J. M. Rost, and S. T. Manson, J. Phys. B **41**, 105101 (2008).
[57] U. Saalmann, C. Siedschlag, and J. M. Rost, J. Phys. B **39**, R39 (2006).
[58] M. J. Puska and R. M. Nieminen, Phys. Rev. A **47**, 1181 (1993).
[59] H. R. Reiss, Phys. Rev. A **75**, 013413 (2007).